Analysis of stability and transition dynamics of skyrmions and skyrmioniums in ferromagnetic nanodisks: A micromagnetic study at finite temperature

Charlie V. Sarmiento* and A. P. Guimarães
Centro Brasileiro de Pesquisas Físicas, Rua Dr. Xavier Sigaud 150, Rio de Janeiro 22290-180, Brazil

(Received 16 March 2024; revised 11 June 2024; accepted 16 August 2024; published 30 August 2024)

Understanding the stability of skyrmions and skyrmioniums is crucial for potential applications, as thermal fluctuations can cause them to transform into other magnetic structures. In this study, we used micromagnetic simulations to examine the regions of stable existence for skyrmion and skyrmionium structures in Co/Pt ferromagnetic nanodisks at 300 K and beyond. We identified stability regions for different values of anisotropy energy (K_z) and interfacial Dzyaloshinskii-Moriya interaction (DMI). Interestingly, these structures share a mutual region of stability. Depending on the thermal energy system, transitions can occur from skyrmionium to skyrmion. We further compute the corresponding thermal activation energy barrier for this transition as $\Delta E/k_B = (15 \pm 2) \times 10^2$ K, with an average lifetime of $\tau_0 = 0.9 \pm 0.4$ ns. This transition can also be triggered by a magnetic field applied along the z-axis.

DOI: 10.1103/PhysRevB.110.064437

I. INTRODUCTION

Skyrmions are distinctive circular magnetic spin nanostructure textures, showing promise for spintronic applications. They are characterized by a quantized topological charge (Q). Their theoretical description of these structures as two-dimensional (2D) localized states in magnetic materials with broken symmetry was first introduced by Bogdanov *et al.* [1,2]. Many years later, the experimental observation of skyrmions was initially achieved through neutron scattering in MnSi [3], $Fe_{1-x}Co_xSi$ [4], and Lorentz transmission electron microscopy in $Fe_{0.5}Co_{0.5}Si$ [5].

In contrast to skyrmions, skyrmioniums are composite structures formed by combining two skyrmions with opposite topological charges. Researchers have explored various methods for stabilizing these structures [6–11], with the interfacial Dzyaloshinskii-Moriya interaction (DMI) emerging as an important stabilizing factor [12–14].

Both skyrmions and skyrmioniums have attracted significant attention due to their promising applications in areas such as logic devices [15,16], microwave devices [17,18], quantum computing [19–22], and neuromorphic computing [23–25].

These structures can be displaced through various methods, including spin-polarized currents [26–29], anisotropy gradients [30], spin waves [31–33], acoustic waves [34], and temperature gradients [35–37]. One crucial distinction between skyrmions and skyrmioniums lies in their response to manipulation. Skyrmions exhibit the skyrmion Hall effect (SkHE), while skyrmioniums do not [38].

For future applications, it is crucial to ensure both stability and controllability of these structures at room temperature [39,40]. This is because different perturbations, such as magnetic fields, spin-polarized currents, thermal fluctuations, and other effects [27,41–47], can trigger transformations from a skyrmion to other magnetic configurations. For such a conversion to take place, it is essential to overcome an energy barrier.

Previous studies involving micromagnetic simulations, atomic simulations, and experimental measurements have investigated the energy barrier required for the transformation of a skyrmion into a ferromagnetic state [46,48–50]. The topological transition from skyrmionium to skyrmion, particularly through the annihilation of its inner core, was first investigated by Hagemeister *et al.* [51] using the geodesic nudged elastic band (GNEB) method. Very recently, Jiang *et al.* [52] explored this transition using micromagnetic theory.

In this study, we conducted micromagnetic simulations by considering a Co/Pt nanodisk to determine if there are regions in the phase diagram of K_z (uniaxial anisotropy) versus DMI where both the skyrmion and the skyrmionium remain stable at room temperature. Based on these results, we calculated the average diameter for both topological structures. Additionally, we computed the energy barrier that has to be overcome to transform a skyrmionium into a skyrmion, as well as the skyrmionium mean lifetime. Subsequently, we constructed a phase diagram that correlates K_z and DMI with the magnetic field strength required to induce the transition.

II. METHODOLOGY

In this study, we made micromagnetic simulations using the MuMax3 program [53]. The simulations were performed considering a ferromagnetic nanodisk of Co/Pt material, with a diameter of 150 nm and a thickness of 1 nm of Co. The cell size was set to $1.0 \times 1.0 \times 1.0$ nm^3. We used the standard magnetic parameters for cobalt (Co) [54,55]: a saturation magnetization (M_s) of 0.58 MA/m, an exchange stiffness constant (A_{ex}) of 15 pJ/m, and a Gilbert damping constant (α) of 0.3. The values of M_s and A_{ex} can be reduced by increasing

*Contact author: charliesarmiento@cbpf.br

the temperature. A comprehensive discussion of this reduction is provided in Sec. 1 of the Supplemental Material [56].

To determine if the magnetic structure (skyrmion and/or skyrmionium) is near a minimum energy, we used the *minimize* command from MuMax3 [66,67]. This approach, employing a steepest-descent method, offers faster convergence compared to the solvers used by the *relax* command. We then verify the structure's stability for a certain time of simulation using the *run* command. All these commands (*minimize*, *relax*, and *run*) perform the numerical integration of the Landau-Lifshitz-Gilbert equation, which is described by

$$\frac{d\mathbf{m}}{dt} = -\gamma_0 \mathbf{m} \times H_{\text{eff}} + \alpha \mathbf{m} \times \frac{d\mathbf{m}}{dt}, \tag{1}$$

where $\mathbf{m}$ represents the vector magnetic moment, $\gamma_0 = 2.211\,05$ m A/s denotes the phenomenological Gilbert damping parameter, and H_{eff} (effective field) is the functional derivative of the energy, given by

$$H_{\text{eff}} = -\frac{1}{\mu_0 M_s} \frac{\delta E}{\delta m}, \tag{2}$$

where M_s is saturation magnetization. The energy contributions in our system of study arise from several sources: Heisenberg exchange interaction, magnetocrystalline anisotropy, Dzyaloshinskii-Moriya interaction. These interactions are specified by phenomenological parameters A_{ex}, K_z, and DMI, respectively. The demagnetization field, arising from the shape of the system and M_s, is automatically calculated within MuMax3. An external magnetic field (H_{ext}) could be added to the effective field. Thermal fluctuations are introduced to the simulation system as a stochastic magnetic field ($\mathbf{H}_{\text{therm}}$) following Brown's model [53,68]. This stochastic field is also implemented in MuMax3 and is described by

$$\mathbf{H}_{\text{therm}} = \boldsymbol{\eta}_{\text{step}} \sqrt{\frac{2\mu_0 \alpha k_B T}{M_s \gamma \Delta V \Delta t}}, \tag{3}$$

where $\boldsymbol{\eta}_{\text{step}}$ is a random vector whose value is changed after every time step, k_B is the Boltzmann constant, T is the temperature, γ is the gyromagnetic ratio, ΔV is the cell volume, and Δt is the time step.

The topological charge (Q) was used to verify the topology of the system and is defined as

$$Q = \frac{1}{4\pi} \int d^2x\, \mathbf{m} \cdot \left(\frac{\partial \mathbf{m}}{\partial x} \times \frac{\partial \mathbf{m}}{\partial y} \right). \tag{4}$$

It was calculated by using the ext_topologicalchargelattice extension implemented in MuMax3, which utilizes the lattice-based approach [53,69].

The analysis of the results obtained through magnetic simulations was conducted using the Python 3.7.11 programming language by utilizing the Pandas 1.3.4 [70], Numpy 1.21.5 [71], and Matplotlib 3.5.3 [72] libraries.

III. RESULTS

A. Stability of skyrmion and skyrmionium

We studied a range of anisotropy energy (K_z) from 0.5 to 1.5 MJ/m^3 and Dzyaloshinskii-Moriya interaction (DMI) from 0.2 to 7.0 mJ/m^2, focusing on regions where these values support the existence of both skyrmion and skyrmionium. However, it is well-established that these structures undergo shape fluctuations due to thermal energy at room temperature, often leading to changes to different magnetic configurations [39].

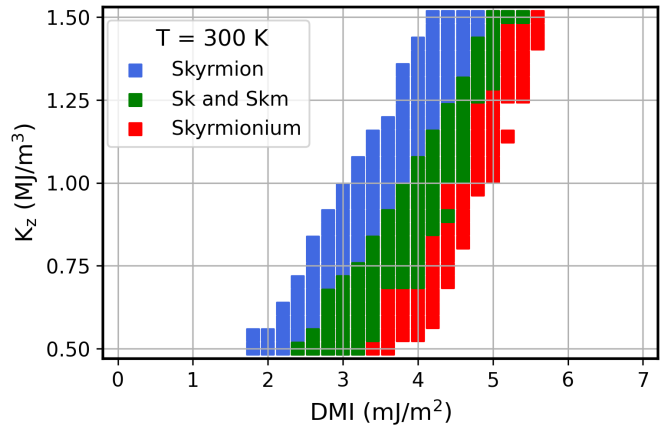

FIG. 1. Phase diagram depicting the stabilization of skyrmions (blue squares), skyrmioniums (red squares), and both structures (green squares) at a temperature of 300 K in the Co/Pt nanodisk.

We determined the regions of stability by following this protocol: each simulation started either with a skyrmion or a skyrmionium configuration. We verified that the magnetic structures were in a minimum energy state using the *minimize* command [66]. Subsequently, we ran the simulations for 1 ns. This allowed us to observe any temperature-induced fluctuations that might occur. We then analyzed the resulting configurations after 1 ns to confirm if the topology remained stable.

Figure 1 shows a phase diagram, where color-coded regions represent the stability of skyrmions (blue), skyrmioniums (red), and the coexistence of both (green) after 1 ns of simulation time. It is important to remark that other magnetic configurations could be stabilized within the depicted K_z and DMI parameter space. For instance, Sec. 2 of the Supplemental Material [56] presents the stability regions of single-domain and multidomain states under the same simulation protocol, but with different initial configuration.

B. Skyrmion and skyrmionium sizes

We determined the diameters of skyrmion and skyrmionium structures from the saved simulation images. Figure 2 presents the results, showing the minimum (a),(c) and mean (b),(d) diameters as a function of K_z (a),(b) for DMI = 5 mJ/m^2, and as a function of DMI (c),(d) for $K_z = 1.5$ MJ/m^3. The minimum diameter is obtained from the image saved immediately after the minimization routine ends, while the mean diameter represents the average value calculated from 20 images saved during the runtime interval.

Previous studies have shown that the diameter of both skyrmions and skyrmioniums increases with increasing DMI, and decreases with increasing K_z (at both 0 K [38] and at finite temperatures [73]). The diameters obtained after the minimization routine agree with this observation. The

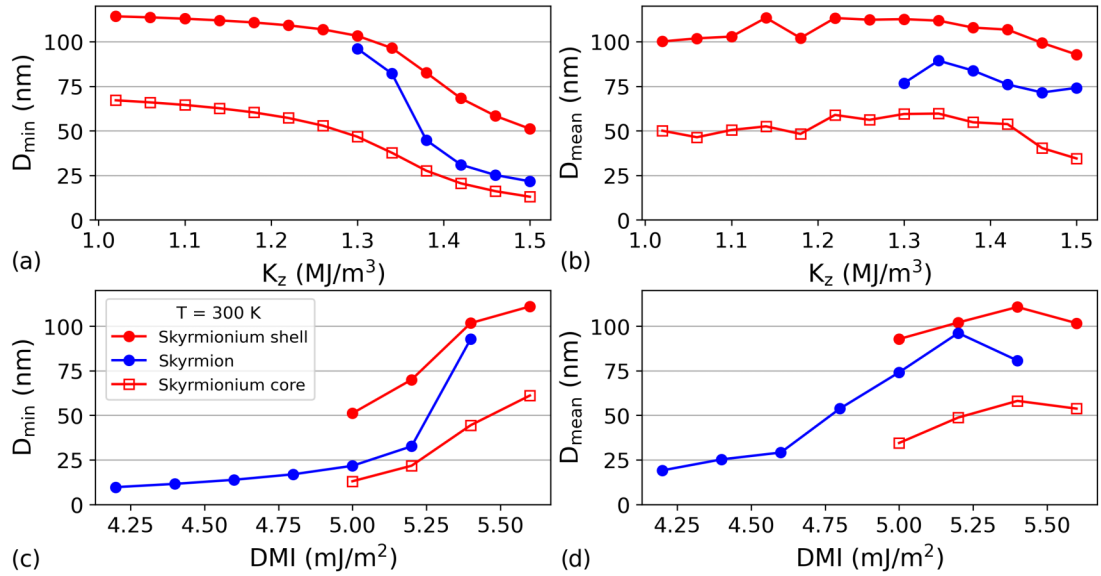

FIG. 2. The diameter of the skyrmion (blue), as well as the core and shell diameters of the skyrmionium (red) vs K_z and DMI at 300 K. The effect of K_z was investigated keeping DMI constant at 5 mJ/m^2 for D_{min} (a),(c) and D_{mean} (b),(d) values, and the effect of varying DMI for a fixed value of K_z (1.5 MJ/m^3).

run command allows us to observe the effects of thermal fluctuations more similar to reality. While the variation in skyrmionium diameter with K_z and DMI is less pronounced within the simulation time frame, we observe that the average diameter D_{mean} remains relatively constant for both skyrmions and skyrmioniums when DMI is held fixed.

Interestingly, the difference in diameters between the core and shell of the skyrmionium remains almost constant as a function of DMI or K_z, considering both the minimum and mean results. This diameter difference is 50 ± 2 nm when DMI is fixed and 48 ± 6 nm for constant K_z, in the case of minimum values. Considering the mean values, this difference is the same for constant DMI and K_z: 51 ± 1 and 51 ± 2 nm, respectively. This characteristic is expected to contribute to the enhanced stability of the skyrmionium, as recently highlighted in the experimental work of Powalla *et al.* [74]. The complete diameter data for skyrmions and skyrmioniums across various K_z and DMI values can be found in Sec. 3 of the Supplemental Material [56].

C. Topological transitions and thermal activation of energy barrier

A simulation time of 1 ns might not be sufficient to definitely assess skyrmion stability. Therefore, we opted to extend the simulation time from 1 to 100 ns, particularly focusing on skyrmionium stability. Within the numerous viable values in the green region of Fig. 1, we selected the specific combination for $K_z = 0.54$ MJ/m^3 and for DMI = 2.6 mJ/m^2. Notably, multiple simulations at 300 K showed no change in the value of the topological charge, which remained near zero (skyrmionium). An attempt was made to detect changes in Q by doing simulations at higher temperatures. Figure 3(a) presents the results of the skyrmionium's topological charge as a function of the simulation time [calculated with Eq. (4)]. The figure shows that at 390 K, Q can exhibit three distinct paths: remaining stable at zero (green line), or fluctuating randomly around 0.3 (orange line, potentially a metastable state), or else fluctuating around 1 (blue line, which represents a skyrmion).

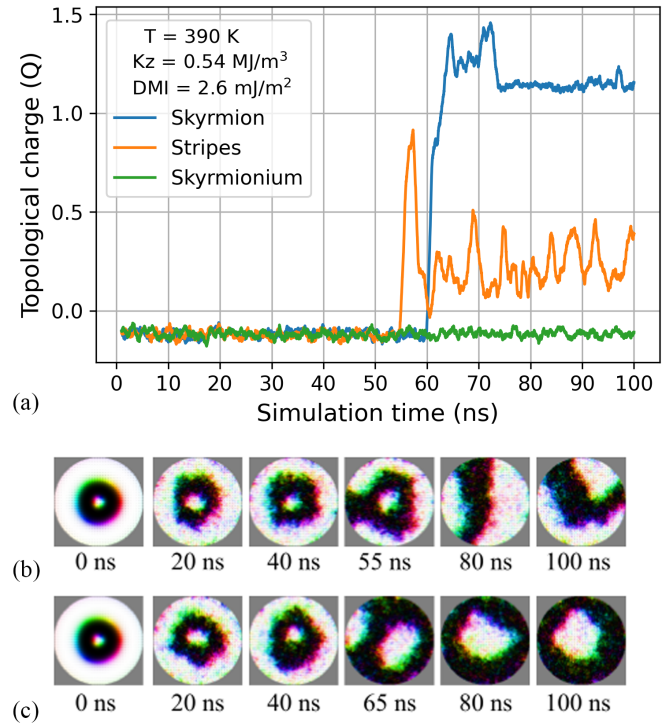

FIG. 3. (a) Mean moving average of the topological charge as a function of time, calculated after the stabilization of a skyrmionium at a temperature of 390 K. The skyrmionium could be stable (green line), or change to a skyrmion (blue line) or change to stripe domains (orange line). Evolution process from skyrmionium (b) into stripe domains, and (c) into a skyrmion.

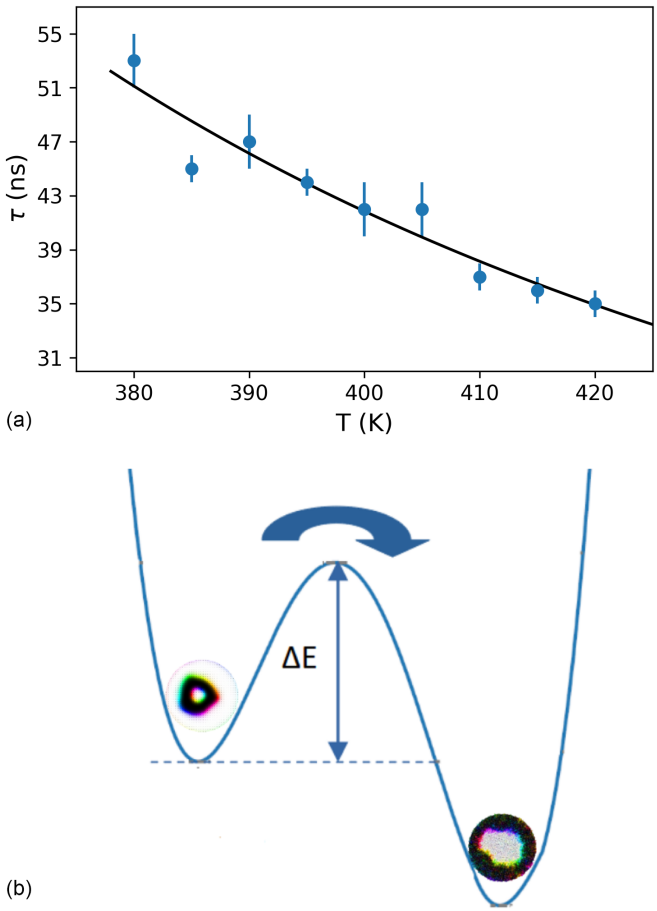

FIG. 4. (a) Relaxation time (τ) as a function of the temperature in the transition from skyrmionium to skyrmion. The energy barrier is $\Delta E/k_B = (15 \pm 2) \times 10^2$ K and $\tau_0 = 0.9 \pm 0.4$ ns. (b) Schematic illustration of the energy minima corresponding to the two configurations.

Figures 3(b) and 3(c) illustrate how the skyrmionium is transformed into a stripe domain (b) and a skyrmion (c) as the simulation time progresses. This transition of the skyrmionium to a skyrmion can be described as radial edgewise, as it involves the gradual fading of the outer part of the skyrmionium at the edge of the nanodisk.

Among the total set of simulations, only about 37% of them exhibited the transitions mentioned. Within this 37%, a mere 7% of the transitions resulted in stripe domains. For the simulations showing the skyrmionium-to-skyrmion transition, we determined the relaxation time by fitting an exponential function (see Sec. 4 of the Supplemental Material [56]). We repeated this process at other temperatures, and the resulting relaxation times are shown in Fig. 4(a).

These relaxation times could be fitted by an exponential function. A schematic illustration of this behavior is depicted in Fig. 4(b), where ΔE is the minimal energy that must be provided to the system if the skyrmionium phase is metastable. This behavior has been previously observed in superparamagnetic systems, including nanoparticles [75,76] and molecular magnets [77,78], and it is usually described by a modified version of Arrhenius' law:

$$\tau = \tau_0 \exp\left(-\Delta E/k_B T\right), \tag{5}$$

where ΔE represents the thermal activation energy or the height of the energy barrier between the two states, τ_0 is the mean lifetime parameter that depends on the nature of the transition, k_B is Boltzmann's constant, and T is the temperature.

The fitting process yielded a thermal barrier height $\Delta E/k_B = (15 \pm 2) \times 10^2$ K and a mean lifetime of $\tau_0 = 0.9 \pm 0.4$ ns. This barrier height is comparable to that reported for the skyrmion-to-ferromagnet transition in other Co/Pt [49,79,80] and PdFe/Ir systems [44,46], obtained through atomistic simulations and experimentally observed in Mn/Si [48]. This result agrees with the idea that a skyrmionium is a composite of two skyrmions with opposite topological charges. In this case, the thermal effect breaks the skyrmionium apart by destroying one of its constituents. In the case of the skyrmionium-to-skyrmion transition, Hagemeister *et al.* [51] found a higher activation energy barrier for the PdFe/Ir system at $T = 0$ K. Conversely, Jiang *et al.* [52] studied the annihilation time of the skyrmionium's center, which is of the order of picoseconds. This is significantly shorter than the nanosecond mean lifetime we observe. This difference could be attributed to the fact that our study deals with the disappearance of the entire outer region of the skyrmionium, as opposed to just a tiny core.

As described in Sec. 1 of the Supplemental Material, a decrease in M_s and A_{ex} is expected with increasing temperature [59]. This reduction is dependent on the thickness of both Co and Pt films. For instance, a sample with a Co film thickness of 1 nm is expected to experience a maximum reduction of 6% in M_s and A_{ex} between 300 and 420 K. This percentage of reduction is not expected to significantly reduce the value of the energy barrier height.

D. Topological transition induced by external magnetic fields

Another method of inducing a topological transition involves the application of a magnetic field. Figure 5 illustrates the variation in Q when a magnetic field is applied along the positive (a) and negative (b) z-axis. The magnetic field was incremented by 0.001 mT every 0.005 ns.

The plots demonstrate that the strength of the magnetic field required to trigger the transition depends on the orientation of the magnetic moments within the nanodisk. A skyrmionium consists of a central core and two encircled rings. The core and the outer ring have magnetic moments pointing in the same direction, while the center ring's moments point in the opposite direction. Domain walls separate these three regions.

In the simulations, the stable skyrmionium has its core magnetic moments pointing in the positive z-axis direction. When a positive field is applied, the domain walls move radially towards the center of the nanodisk, collapsing the core region into a Bloch point (a specific magnetic configuration with three magnetic moments). This behavior is consistent with findings by Hagemeister *et al.* [51]. Conversely, when the magnetic field is applied in the opposite direction, the domain walls move radially away from the center of the nanodisk,

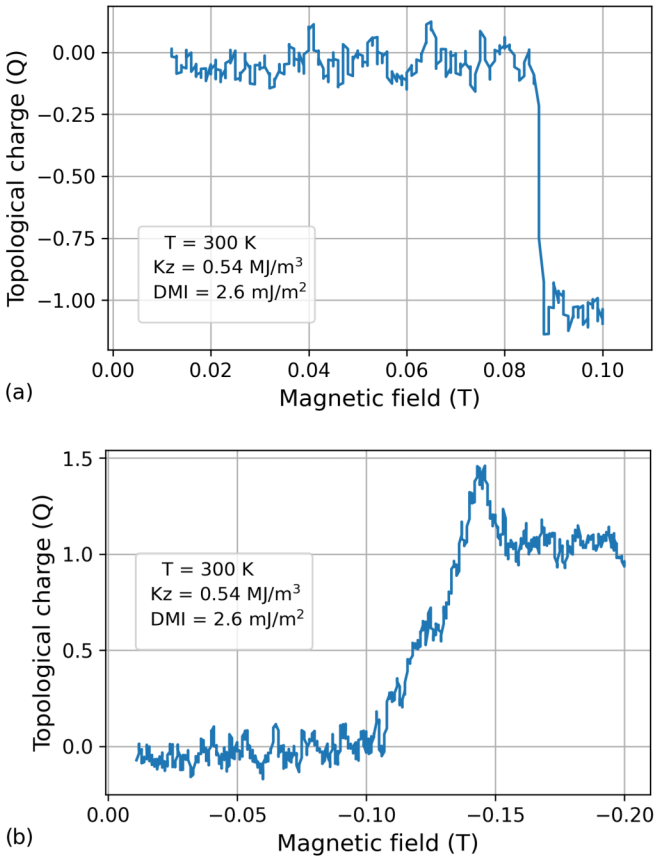

FIG. 5. Topological charge vs magnetic field applied (a) in the positive direction and (b) in the negative direction of the z-axis.

similar to the behavior depicted in Fig. 3(c). As is evident from Figs. 5(a) and 5(b), the field's effect is clearly dependent on its direction.

For the selected values of K_z and DMI, inducing outward radial movement of the domain walls proves more challenging. Additionally, the transition could either occur suddenly or require a more extended application of the magnetic field, and these variations are attributable to thermal fluctuations. As the domain walls shift outwards from the rim of the nanodisk, the outermost part of the skyrmionium is gradually removed, while in the case of inward movement, the core of the skyrmionium eventually becomes a Bloch point.

We then applied a series of linear magnetic fields to all possible combinations of K_z and DMI values within the green region of Fig. 1, where both skyrmionium and skyrmion remained stable at 300 K. This approach enabled us to ascertain the strength of a positive z-axis magnetic field required to induce the skyrmionium-to-skyrmion transition for each K_z and DMI combination. The results are visualized in Fig. 6 as a color map, where each color (ranging from creamy yellow to black) represents the magnetic field strength required for the transition. The color-scale key mapping these values is provided on the right side of the graph.

Analyzing these values, we observed a range of magnetic field strengths required for the transition, with a minimum of 0.076 T (at $K_z = 0.50$ MJ/m^3 and DMI $= 2.4$ mJ/m^2), and a maximum of 0.360 T (at $K_z = 1.02$ MJ/m^3 and DMI $= 4.8$ mJ/m^2). These results suggest that the energy

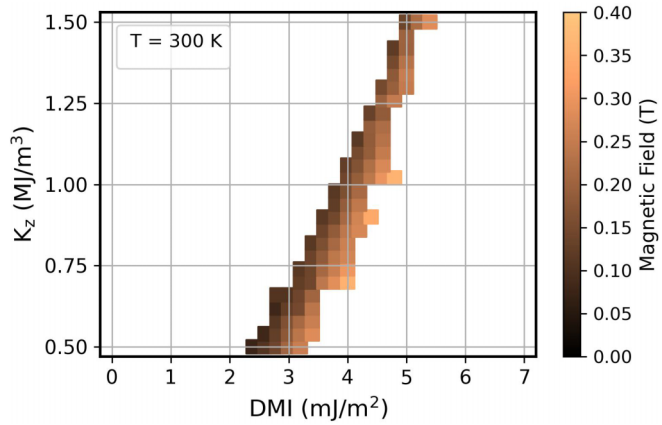

FIG. 6. Phase diagram of K_z vs DMI, illustrating the magnetic field strength required to induce the topological transition when applied along the z-axis.

barrier height between skyrmionium and skyrmion for the latter case could be up to five times higher than the value determined in the previous section. Notably, it is apparent that lower values of K_z and DMI require a lower magnetic field for the topological transition. Interestingly, the highest magnetic field value was not observed at the extreme K_z and DMI values but rather at intermediate values.

IV. CONCLUSIONS

We investigated the stability of skyrmioniums and skyrmions in a Co/Pt nanodisk using micromagnetic simulations. We identified a region of K_z and DMI values where both structures are stable at room temperature (300 K), defining a region of mutual stability.

With the objective of determining the maximum temperature at which skyrmioniums remain stable, more simulations were performed at higher temperatures. These simulations revealed specific temperatures where skyrmioniums undergo thermally driven topological transitions following a Markovian process. Subsequently, we calculated the relaxation times at nine distinct temperatures ranging from 380 to 420 K. Our analysis revealed that these results follow Arrhenius law, leading us to determine the thermal activation energy barrier between skyrmionium and skyrmion, as $\Delta E/k_B = (15 \pm 2) \times 10^2$ K. Notably, this activation energy is in the same range of values observed in the transition from a skyrmion to a ferromagnetic state in different ferromagnetic systems. However, the energy barrier height is dependent on the thickness of Co and Pt films, and it can also be tailored by incorporating different materials.

Different types of perturbations can induce the observed transition from skyrmionium to skyrmion. For simplicity, we employed magnetic fields that varied linearly with time to induce this transition. By doing so, we determined the field strength required to induce this topological transition for each pair of K_z and DMI values, where these topologies are stable. These findings suggest the presence of points on the phase diagram that may exhibit energy barriers higher than the one that was determined.

ACKNOWLEDGMENTS

The authors would like to thank Dr. H. Vigo-Cotrina for his support during the process of data analysis. The authors are grateful to the Brazilian Center for Research in Physics (CBPF) for providing access to their computing facilities. Finally, the authors would like to acknowledge the support of the "Programa de Capacitação Institucional" (PCI) financed by the "Ministério da Ciência, Tecnologia e Inovação" (MCTI).

[1] A. N. Bogdanov and D. A. Yablonskii, Thermodynamically stable "vortices" in magnetically ordered crystals. The mixed state of magnets, Sov. Phys. JETP **68**, 101 (1989).

[2] A. Bogdanov and C. Panagopoulos, Physical foundations and basic properties of magnetic skyrmions, Nat. Rev. Phys. **2**, 492 (2020).

[3] S. Mühlbauer, B. Binz, F. Jonietz, C. Pfleiderer, A. Rosch, A. Neubauer, R. Georgii, and P. Böni, Skyrmion lattice in a chiral magnet, Science **323**, 915 (2009).

[4] W. Münzer, A. Neubauer, T. Adams, S. Mühlbauer, C. Franz, F. Jonietz, R. Georgii, P. Böni, B. Pedersen, M. Schmidt *et al.*, Skyrmion lattice in the doped semiconductor $Fe_{1-x}Co_xSi$, Phys. Rev. B **81**, 041203(R) (2010).

[5] X. Yu, Y. Onose, N. Kanazawa, J. Park, J. Han, Y. Matsui, N. Nagaosa, and Y. Tokura, Real-space observation of a two-dimensional skyrmion crystal, Nature (London) **465**, 901 (2010).

[6] S. Heinze, K. Von Bergmann, M. Menzel, J. Brede, A. Kubetzka, R. Wiesendanger, G. Bihlmayer, and S. Blügel, Spontaneous atomic-scale magnetic skyrmion lattice in two dimensions, Nat. Phys. **7**, 713 (2011).

[7] T. Okubo, S. Chung, and H. Kawamura, Multiple-q states and the skyrmion lattice of the triangular-lattice Heisenberg antiferromagnet under magnetic fields, Phys. Rev. Lett. **108**, 017206 (2012).

[8] S. A. Montoya, S. Couture, J. J. Chess, J. C. T. Lee, N. Kent, D. Henze, S. K. Sinha, M.-Y. Im, S. D. Kevan, P. Fischer *et al.*, Tailoring magnetic energies to form dipole skyrmions and skyrmion lattices, Phys. Rev. B **95**, 024415 (2017).

[9] T. Garel and S. Doniach, Phase transitions with spontaneous modulation-the dipolar Ising ferromagnet, Phys. Rev. B **26**, 325 (1982).

[10] Y. Lin, P. Grundy, and E. Giess, Bubble domains in magnetostatically coupled garnet films, Appl. Phys. Lett. **23**, 485 (1973).

[11] N. Nagaosa and Y. Tokura, Topological properties and dynamics of magnetic skyrmions, Nat. Nanotechnol. **8**, 899 (2013).

[12] I. Dzyaloshinsky, A thermodynamic theory of "weak" ferromagnetism of antiferromagnetics, J. Phys. Chem. Solids **4**, 241 (1958).

[13] T. Moriya, Anisotropic superexchange interaction and weak ferromagnetism, Phys. Rev. **120**, 91 (1960).

[14] X. Liu, Q. Zhu, S. Zhang, Q. Liu, and J. Wang, Static property and current-driven precession of 2π-vortex in nano-disk with Dzyaloshinskii-Moriya interaction, AIP Adv. **5**, 087137 (2015).

[15] X. Zhang, Y. Zhou, M. Ezawa, G. Zhao, and W. Zhao, Magnetic skyrmion transistor: Skyrmion motion in a voltage-gated nanotrack, Sci. Rep. **5**, 11369 (2015).

[16] S. Luo, M. Song, X. Li, Y. Zhang, J. Hong, X. Yang, X. Zou, N. Xu, and L. You, Reconfigurable skyrmion logic gates, Nano Lett. **18**, 1180 (2018).

[17] W. Wang, M. Beg, B. Zhang, W. Kuch, and H. Fangohr, Driving magnetic skyrmions with microwave fields, Phys. Rev. B **92**, 020403(R) (2015).

[18] J. Xia, Y. Huang, X. Zhang, W. Kang, C. Zheng, X. Liu, W. Zhao, and Y. Zhou, A microwave field-driven transistor-like skyrmionic device with the microwave current-assisted skyrmion creation, J. Appl. Phys. **122**, 153901 (2017).

[19] M. Chauwin, X. Hu, F. Garcia-Sanchez, N. Betrabet, A. Paler, C. Moutafis, and J. S. Friedman, Skyrmion logic system for large-scale reversible computation, Phys. Rev. Appl. **12**, 064053 (2019).

[20] S. Li, W. Kang, X. Zhang, T. Nie, Y. Zhou, K. Wang, and W. Zhao, Magnetic skyrmions for unconventional computing, Mater. Horiz. **8**, 854 (2021).

[21] T. Weber, D. Fobes, J. Waizner, P. Steffens, G. Tucker, M. Böhm, L. Beddrich, C. Franz, H. Gabold, R. Bewley *et al.*, Topological magnon band structure of emergent Landau levels in a skyrmion lattice, Science **375**, 1025 (2022).

[22] Z. Li, M. Ma, Z. Chen, K. Xie, and F. Ma, Interaction between magnon and skyrmion: Toward quantum magnonics, J. Appl. Phys. **132**, 210702 (2022).

[23] S. Li, A. Du, Y. Wang, X. Wang, X. Zhang, H. Cheng, W. Cai, S. Lu, K. Cao, B. Pan *et al.*, Experimental demonstration of skyrmionic magnetic tunnel junction at room temperature, Sci. Bull. **67**, 691 (2022).

[24] S. Saini, N. Bindal, and B. Kaushik, Skyrmionium-based leaky integrate and fire neuron, in *Proceedings of the IEEE 23rd International Conference on Nanotechnology (NANO)*, *Jeju City, Republic of Korea* (IEEE, Piscataway, NJ, 2023), pp. 209–214.

[25] Z. Hou, Y. Wang, X. Lan, S. Li, X. Wan, F. Meng, Y. Hu, Z. Fan, C. Feng, M. Qin *et al.*, Controlled switching of the number of skyrmions in a magnetic nanodot by electric fields, Adv. Mater. **34**, 2107908 (2022).

[26] C. Deger, I. Yavuz, and F. Yildiz, Current-driven coherent skyrmion generation, Sci. Rep. **9**, 3513 (2019).

[27] S.-Z. Lin, C. Reichhardt, C. D. Batista, and A. Saxena, Driven skyrmions and dynamical transitions in chiral magnets, Phys. Rev. Lett. **110**, 207202 (2013).

[28] Y. Liu, H. Du, M. Jia, and A. Du, Switching of a target skyrmion by a spin-polarized current, Phys. Rev. B **91**, 094425 (2015).

[29] W. Farias, I. Santece, and P. Coura, The influence of curved surfaces on the propagation of skyrmions in a magnetic racetrack, J. Magn. Magn. Mater. **568**, 170386 (2023).

[30] R. Tomasello, S. Komineas, G. Siracusano, M. Carpentieri, and G. Finocchio, Chiral skyrmions in an anisotropy gradient, Phys. Rev. B **98**, 024421 (2018).

[31] S. Li, J. Xia, X. Zhang, M. Ezawa, W. Kang, X. Liu, Y. Zhou, and W. Zhao, Dynamics of a magnetic skyrmionium driven by spin waves, Appl. Phys. Lett. **112**, 142404 (2018).

[32] M. Shen, Y. Zhang, J. Ou-Yang, X. Yang, and L. You, Motion of a skyrmionium driven by spin wave, Appl. Phys. Lett. **112**, 062403 (2018).

[33] J. Ding, X. Yang, and T. Zhu, The motion of magnetic skyrmions driven by propagating spin waves, IEEE Trans. Magn. **51**, 1 (2015).

[34] J. Sun, Y. Zhao, S. Shi, Y. Zhang, and J. Wang, Motion of a magnetic skyrmionium driven by acoustic wave, Appl. Phys. Lett. **121**, 242406 (2022).

[35] S.-Z. Lin, C. D. Batista, C. Reichhardt, and A. Saxena, AC current generation in chiral magnetic insulators and skyrmion motion induced by the spin Seebeck effect, Phys. Rev. Lett. **112**, 187203 (2014).

[36] A. A. Kovalev, Skyrmionic spin Seebeck effect via dissipative thermomagnonic torques, Phys. Rev. B **89**, 241101(R) (2014).

[37] C. Gong, Y. Zhou, and G. Zhao, Dynamics of magnetic skyrmions under temperature gradients, Appl. Phys. Lett. **120**, 052402 (2022).

[38] A. Kolesnikov, M. Stebliy, A. Samardak, and A. Ognev, Skyrmionium–high velocity without the skyrmion Hall effect, Sci. Rep. **8**, 16966 (2018).

[39] J. Wang, M. Strungaru, S. Ruta, A. Meo, Y. Zhou, A. Deák, L. Szunyogh, P. Gavriloaea, R. Moreno, O. Chubykalo-Fesenko *et al.*, Spontaneous creation and annihilation dynamics of magnetic skyrmions at elevated temperature, Phys. Rev. B **104**, 054420 (2021).

[40] J. Wang, J. Xia, X. Zhang, X. Zheng, G. Li, L. Chen, Y. Zhou, J. Wu, H. Yin, R. Chantrell *et al.*, Magnetic skyrmionium diode with a magnetic anisotropy voltage gating, Appl. Phys. Lett. **117**, 202401 (2020).

[41] S. Yang, Y. Zhao, K. Wu, Z. Chu, X. Xu, X. Li, J. Åkerman, and Y. Zhou, Reversible conversion between skyrmions and skyrmioniums, Nat. Commun. **14**, 3406 (2023).

[42] L. Bo, R. Zhao, C. Hu, Z. Shi, W. Chen, X. Zhang, and M. Yan, Formation of skyrmion and skyrmionium in confined nanodisk with perpendicular magnetic anisotropy, J. Phys. D **53**, 195001 (2020).

[43] H. Vigo-Cotrina and A. Guimarães, Creating skyrmions and skyrmioniums using oscillating perpendicular magnetic fields, J. Magn. Magn. Mater. **507**, 166848 (2020).

[44] P. Bessarab, G. Müller, I. Lobanov, F. Rybakov, N. Kiselev, H. Jónsson, V. Uzdin, S. Blügel, L. Bergqvist, and A. Delin, Lifetime of racetrack skyrmions, Sci. Rep. **8**, 3433 (2018).

[45] S. von Malottki, B. Dupé, P. Bessarab, A. Delin, and S. Heinze, Enhanced skyrmion stability due to exchange frustration, Sci. Rep. **7**, 12299 (2017).

[46] L. Rózsa, E. Simon, K. Palotás, L. Udvardi, and L. Szunyogh, Complex magnetic phase diagram and skyrmion lifetime in an ultrathin film from atomistic simulations, Phys. Rev. B **93**, 024417 (2016).

[47] Y. Zhou and M. Ezawa, A reversible conversion between a skyrmion and a domain-wall pair in a junction geometry, Nat. Commun. **5**, 4652 (2014).

[48] H. Oike, A. Kikkawa, N. Kanazawa, Y. Taguchi, M. Kawasaki, Y. Tokura, and F. Kagawa, Interplay between topological and thermodynamic stability in a metastable magnetic skyrmion lattice, Nat. Phys. **12**, 62 (2016).

[49] S. Rohart, J. Miltat, and A. Thiaville, Path to collapse for an isolated Néel skyrmion, Phys. Rev. B **93**, 214412 (2016).

[50] C. Schütte and A. Rosch, Dynamics and energetics of emergent magnetic monopoles in chiral magnets, Phys. Rev. B **90**, 174432 (2014).

[51] J. Hagemeister, A. Siemens, L. Rózsa, E. Vedmedenko, and R. Wiesendanger, Controlled creation and stability of k π skyrmions on a discrete lattice, Phys. Rev. B **97**, 174436 (2018).

[52] A. Jiang, Y. Zhou, X. Zhang, and M. Mochizuki, Transformation of a skyrmionium to a skyrmion through the thermal annihilation of the inner skyrmion, Phys. Rev. Res. **6**, 013229 (2024).

[53] A. Vansteenkiste, J. Leliaert, M. Dvornik, M. Helsen, F. Garcia-Sanchez, and B. Van Waeyenberge, The design and verification of MuMax3, AIP Adv. **4**, 107133 (2014).

[54] H. Vigo-Cotrina, D. Monteiro, J. Urruchua, and A. Guimarães, The emergence of kπ skyrmions and their spin wave modes in a ferromagnetic disk, J. Magn. Magn. Mater. **560**, 169665 (2022).

[55] J. Sampaio, V. Cros, S. Rohart, A. Thiaville, and A. Fert, Nucleation, stability and current-induced motion of isolated magnetic skyrmions in nanostructures, Nat. Nanotechnol. **8**, 839 (2013).

[56] See Supplemental Material at http://link.aps.org/supplemental/10.1103/PhysRevB.110.064437 for additional details: Sec. 1 provides a comprehensive description of the temperature dependence of relevant magnetic parameters, which includes Refs. [57–65]; Sec. 2 presents a figure illustrating the stability regions of single-domain and multidomain structures; Sec. 3 includes a figure composed of six subfigures, which offer magnified views of the results shown in Fig. 2 of the main text; Sec. 4 contains a figure comprising nine subfigures, each displaying the exponential fit to survival statistics at various temperatures as a function of simulation time.

[57] G. Riley, J. Shaw, T. Silva, and H. Nembach, Simultaneous measurement of the exchange parameter and saturation magnetization using propagating spin waves, Appl. Phys. Lett. **120**, 112405 (2022).

[58] S. Schlotter, P. Agrawal, and G. Beach, Temperature dependence of the Dzyaloshinskii-Moriya interaction in Pt/Co/Cu thin film heterostructures, Appl. Phys. Lett. **113**, 092402 (2018).

[59] H. W. van Kesteren and W. Zeper, Controlling the Curie temperature of Co/Pt multilayer magneto-optical recording media, J. Magn. Magn. Mater. **120**, 271 (1993).

[60] C. Eyrich, A. Zamani, W. Huttema, M. Arora, D. Harrison, F. Rashidi, D. Broun, B. Heinrich, O. Mryasov, M. Ahlberg, O. Karis, P. E. Jönsson, M. From, X. Zhu, and E. Girt, Effects of substitution on the exchange stiffness and magnetization of Co films, Phys. Rev. B **90**, 235408 (2014).

[61] N. Inaba, Y. Uesaka, and M. Futamoto, Compositional and temperature dependence of basic magnetic properties of CoCr-alloy thin films, IEEE Trans. Magn. **36**, 54 (2000).

[62] Y. Tserkovnyak, A. Brataas, and G. Bauer, Spin pumping and magnetization dynamics in metallic multilayers, Phys. Rev. B **66**, 224403 (2002).

[63] T. Verhagen, H. Tinkey, H. Overweg, M. Van Son, M. Huber, J. Van Ruitenbeek, and J. Aarts, Temperature dependence of spin pumping and Gilbert damping in thin Co/Pt bilayers, J. Phys.: Condens. Matter **28**, 056004 (2016).

[64] Y. Tserkovnyak, A. Brataas, G. Bauer, and B. Halperin, Nonlocal magnetization dynamics in ferromagnetic heterostructures, Rev. Mod. Phys. **77**, 1375 (2005).

[65] Y. Liu, P. Yang, and P. Kelly, Gilbert damping for magnetic multilayers with perpendicular magnetic anisotropy, Phys. Rev. B **109**, 014416 (2024).

[66] J. J. Joos, P. Bassirian, P. Gypens, J. Mulkers, K. Litzius, B. Van Waeyenberge, and J. Leliaert, Tutorial: Simulating modern magnetic material systems in mumax3, J. Appl. Phys. **134**, 171101 (2023).

[67] L. Exl, S. Bance, F. Reichel, T. Schrefl, H. Peter Stimming, and N. Mauser, LaBonte's method revisited: An effective steepest descent method for micromagnetic energy minimization, J. Appl. Phys. **115**, 17D118 (2014).

[68] W. F. Brown, Thermal fluctuations of a single-domain particle, Phys. Rev. **130**, 1677 (1963).

[69] J. Kim and J. Mulkers, On quantifying the topological charge in micromagnetics using a lattice-based approach, IOP SciNotes **1**, 025211 (2020).

[70] W. McKinney, S. Walt, and J. Millman, in *Proceedings of the 9th Python in Science Conference, Austin, Texas, 2010* (SciPy, 2010).

[71] C. Harris, K. Millman, S. Van Der Walt, R. Gommers, P. Virtanen, D. Cournapeau, E. Wieser, J. Taylor, S. Berg, N. Smith *et al.*, Array programming with NumPy, Nature (London) **585**, 357 (2020).

[72] J. Hunter, Matplotlib: A 2D graphics environment, Comput. Sci. Eng. **9**, 90 (2007).

[73] C. Moreau-Luchaire, C. Moutafis, N. Reyren, J. Sampaio, C. Vaz, N. Van Horne, K. Bouzehouane, K. Garcia, C. Deranlot, P. Warnicke *et al.*, Additive interfacial chiral interaction in multilayers for stabilization of small individual skyrmions at room temperature, Nat. Nanotechnol. **11**, 444 (2016).

[74] L. Powalla, M. Birch, K. Litzius, S. Wintz, F. Yasin, L. Turnbull, F. Schulz, D. Mayoh, G. Balakrishnan, M. Weigand *et al.*, Seeding and emergence of composite skyrmions in a van der Waals magnet, Adv. Mater. **35**, 2208930 (2023).

[75] L. Nagy, A. Zeleňáková, J. Szűcsová, N. Mielnik, and P. Hrubovčák, Characterization of cobalt ferrite magnetic nanoparticles for magnetic hyperthermia application, AIP Conf. Proc. **2778**, 040020 (2023).

[76] G. Barrera, P. Allia, and P. Tiberto, Temperature-dependent heating efficiency of magnetic nanoparticles for applications in precision nanomedicine, Nanoscale **12**, 6360 (2020).

[77] Z. Yang, F. Gong, D. Lin, and Y. Huo, Recent advances in polyoxometalate-based single-molecule magnets, Coord. Chem. Rev. **492**, 215205 (2023).

[78] E. Coronado, Molecular magnetism: From chemical design to spin control in molecules, materials and devices, Nat. Rev. Mater. **5**, 87 (2020).

[79] I. Lobanov, H. Jónsson, and V. Uzdin, Mechanism and activation energy of magnetic skyrmion annihilation obtained from minimum energy path calculations, Phys. Rev. B **94**, 174418 (2016).

[80] D. Cortés-Ortuño, W. Wang, M. Beg, R. Pepper, M. Bisotti, R. Carey, M. Vousden, T. Kluyver, O. Hovorka, and H. Fangohr, Thermal stability and topological protection of skyrmions in nanotracks, Sci. Rep. **7**, 4060 (2017).